Graph-based Multivariate Multiscale Permutation Entropy: Study of Robustness to Noise and Application to Two-Phase Flow Data

John Stewart Fabila-Carrasco
School of Engineering
University of Edinburgh, UK.
Institute for Digital Communications
Edinburgh, EH9 3FB, UK
john.fabila@ed.ac.uk

Chao Tan
School of Electrical and Information Engineering
Tianjin University
Tianjin, 300072, China
tanchao@tju.edu.cn

Javier Escudero
School of Engineering
University of Edinburgh, UK.
Institute for Digital Communications
Edinburgh, EH9 3FB, UK
javier.escudero@ed.ac.uk

***Abstract*—We propose a novel technique for exploring the complexity of multivariate time series (possibly with different lengths) across multiple time scales using a new graph-based approach. Our method, called multivariate multiscale permutation entropy, $\mathrm{MMPE_G}$, incorporates the interactions between channels by constructing an underlying graph for each coarse-grained time series and then applying the recent permutation entropy for graph signals. This approach enables the analysis of multivariate time series with varying lengths, providing insights into the dynamics and relationships between different channels.**

To address the challenge posed by noise in real-world data analysis, we evaluate the robustness of $\mathrm{MMPE_G}$ to noise using synthetic time series with varying levels of noise. Our results show that $\mathrm{MMPE_G}$ exhibits better performance than similar multivariate entropy metrics.

We also apply $\mathrm{MMPE_G}$ to study two-phase flow data, an important industrial process characterised by complex and dynamic behaviour. Specifically, we process multivariate Electrical Resistance Tomography (ERT) data and extract multivariate multiscale permutation entropy values. The results indicate that $\mathrm{MMPE_G}$ characterises the flow behaviour transition of two-phase flow by incorporating information from different scales and is sensitive to the dynamics of different flow patterns. The noise-robustness of $\mathrm{MMPE_G}$ makes it a suitable approach for analysing the complexity of multivariate time series and characterising two-phase flow recordings.

***Index Terms*—dispersion entropy, complexity, graph signals, entropy metrics, two-phase flow, multivariate time series**

I. Introduction

Two-phase flow is a critical phenomenon in various industrial applications, including chemical processes, petroleum exploitation, and nuclear engineering [1]. Despite extensive research on two-phase flow, including theoretical and experimental studies employing mathematical approaches [2], [3], and high-speed camera techniques [4], the complexity and dynamic behaviours of the flow patterns, particularly in the interaction between different channels in the multivariate recordings, remain unresolved. Accurate characterization of two-phase flow can lead to improved efficiency, reduced costs, and sustainable development [1].

Non-linear analysis metrics can be useful for studying complex systems, such as two-phase flow. Univariate permutation entropy [5], a computationally efficient non-linear measure of complexity, has been employed for characterizing various systems. Its performance under noisy conditions has been investigated [6], and it has been used to distinguish two-phase flow dynamics [7] and characterize autoregressive processes [8]. However, most physical systems' signals are multivariate. Therefore, several univariate entropy metrics have been extended to a multivariate setting, including multivariate generalisations of sample entropy [9], dispersion entropy [10], and permutation entropy [11], among others. Some of these methods have been recently used to analyse two-phase flow and characterize its behaviour [12]–[14]. However, prior implementations of multivariate permutation entropy are limited as they do not consider cross-channel information, exhibit limitations in noise robustness and complexity capture, particularly in the context of two-phase flow data.

Noise can impact the accuracy of multivariate entropy metrics, leading to inaccurate values. Several techniques, such as multivariate weighted permutation entropy [15], have been proposed to address this issue. However, these multivariate methods analyse each time series separately, leading to the loss of cross-channel information and an increase in the number of parameters used for entropy computation. To address these limitations, we propose a multiscale multivariate permutation entropy, $\mathrm{MMPE_G}$, based on a general graph construction (and not limited to the Cartesian graph product [16], which requires equal length time series). Our method, $\mathrm{MMPE_G}$, can identify patterns in two-phase flow data that are not discernible through traditional time series entropies or statistical analysis, making it a valuable tool for the characterization of these systems.

Contributions: We introduce a multiscale algorithm for analysing multivariate time series based on permutation entropy for graph signals ($\mathrm{PE_G}$). We apply the algorithm to a set of synthetic data and two-phase flow data, demonstrating

This work was supported by the Leverhulme Trust via a Research Project Grant (RPG-2020-158).

that it outperforms univariate permutation entropy and classical multivariate permutation entropy. Our method, $\mathrm{MMPE_G}$, considers the interaction between different data channels, is robust to noise, and detects complexity at different scales of the two-phase flow patterns. Furthermore, the generality of the construction of the underlying graph allows for the treatment of not only multivariate and multiscale time series but also other types of data, such as irregularly sampled time series. This includes channels with varying levels of importance (by incorporating a weighted adjacency matrix) or channels with unequal lengths, thereby enabling the application of $\mathrm{PE_G}$ to cases where this was not previously possible. Overall, $\mathrm{MMPE_G}$ presents distinct advantages over existing methods. Its enhanced noise robustness, a critical attribute for real-world data analysis, and sensitivity to diverse dynamics facilitate here its application to differentiate multi-phase flow patterns, achieving a notable improvement over previous methods.

II. Graphs and permutation entropy

This section presents the Cartesian graph product and the permutation entropy for analyse graph signals, defined in [17].

Cartesian graph product. The *Cartesian product* of two graphs $G = (\mathcal{V}, \mathcal{E})$ and $G' = (\mathcal{V}', \mathcal{E}')$, denoted $G \square G'$, is the graph defined by the vertex set: $\mathcal{V}(G \square G') = \mathcal{V} \times \mathcal{V}' = \{\, (v, v') \,|\, v \in \mathcal{V} \text{ and } v' \in \mathcal{V}' \,\}$. Two vertices (v, v') and (u, u') are adjacent in $G \square G'$ if and only if either $v = u$ and v' is adjacent to u' in G', or $v' = u'$ and v is adjacent to u in G. The graph product is a useful structure to model multidomain signals [18] and is the perturbation of a periodic graph [19].

Permutation entropy for graph signals ($\mathrm{PE_G}$). Let $G = (\mathcal{V}, \mathcal{E})$ be a graph, $\mathbf{A}$ its adjacency matrix and $\mathbf{X} = \{x_i\}_{i=1}^{n}$ be a signal on the graph, $\mathrm{PE_G}$ is defined in [16], [17] as follows:
1) For $2 \leq m \in \mathbb{N}$ the *embedding dimension*, $L \in \mathbb{N}$ the *delay time* and for all $i = 1, 2, \ldots, n$, we define $y_i^{kL} = \frac{1}{|\mathcal{N}_{kL}(i)|} \sum_{j \in \mathcal{N}_{kL}(i)} x_j = \frac{1}{|\mathcal{N}_{kL}(i)|} (\mathbf{A}^{kL}\mathbf{X})_i$, where $\mathcal{N}_k(i) = \{\, j \in \mathcal{V} \,|\, \text{it exists a walk on } k \text{ edges joining } i \text{ and } j \,\}$. Then, we construct the embedding vector $\mathbf{y}_i^{m,L} \in \mathbb{R}^m$ given by

$$\mathbf{y}_i^{m,L} = \left(y_i^{kL}\right)_{k=0}^{m-1} = \left(y_i^0, y_i^L, \ldots y_i^{(m-1)L}\right) \ .$$

2) The embedding vector $\mathbf{y}_i^{m,L}$ is arranged in increasing order and is assigned to one of $k = m!$ permutation (or patterns) $\pi_1, \pi_2, \ldots, \pi_k$.
3) For the distinct permutation, the relative frequency is denoted by $p(\pi_1), p(\pi_2), \ldots, p(\pi_k)$. The permutation entropy $\mathrm{PE_G}$ for the graph signal $\mathbf{X}$ is computed as the normalised Shannon entropy

$$\mathrm{PE_G} = -\frac{1}{\ln(m!)} \sum_{i=1}^{m!} p(\pi_i) \ln p(\pi_i) \ .$$

III. Multiscale Multivariate Permutation Entropy ($\mathrm{MMPE_G}$)

Time series from phase flow data contain multiple temporal scale structures. A single scale can only assess the system's irregularity at a single temporal scale. Multiple scales need to be analysed to understand the dynamics in the signals and to describe the properties of its model. Here, we propose a nonlinear multivariate multiscale methodology based on graph signals to analyse such data.

Let $\mathbf{X} = \{x_{t,s}\}_{t=1,2,\ldots,n_p}^{s=1,2,\ldots,p}$ be a multivariate time series with $p-$channels, each of length n_p and I_p be the graph of interactions between channels. The $\mathrm{MMPE_G}$ algorithm relies on a three-step procedure:

1) **Coarse-grained procedure.** From the original multivariate signal $\mathbf{X}$, we derive multiple successive coarse-grained versions by averaging the time data points within non-overlapping time segments of increasing length, ϵ , referred to as the scale factor. Each element of the coarse-grained time series,

$$\mathbf{U}^\epsilon = \{u_{i,j}^\epsilon\}_{i=1,2,\ldots,\lfloor n_p/\epsilon \rfloor}^{j=1,2,\ldots,p} \ ; \tag{1}$$

where each $u_{i,j}^\epsilon$ is calculated as:

$$u_{i,j}^\epsilon = \frac{1}{\epsilon} \sum_{t=(i-1)\epsilon+1}^{i\epsilon} x_{t,j} \ , \quad \text{for } 1 \leq j \leq p \text{ and } 1 \leq i \leq n_p/\epsilon \ .$$

2) **Graph construction associated to a multivariate signal.** For each coarse-grained multivariate $\mathbf{U}^\epsilon$ (Eq. 1), we construct the graph $\mathcal{G}_{\mathbf{U}^\epsilon} = (\mathcal{V}, \mathcal{E})$ as follows:

- The vertex set $\mathcal{V} = \{v_{i,j}^\epsilon\}_{i=1,2,\ldots,\lfloor n_p/\epsilon \rfloor}^{j=1,2,\ldots,p}$.
- The edge set $\mathcal{E} = \mathcal{E}_1 \cup \mathcal{E}_2$ where

$$\mathcal{E}_1 = \{\, \left(v_{i,j}^\epsilon, v_{i+1,j}^\epsilon\right) \,|\, 1 \leq i \leq \lfloor n_p/\epsilon \rfloor - 1 \,\} \ ,$$
$$\mathcal{E}_2 = \{\, \left(v_{i,j}^\epsilon, v_{k,j}^\epsilon\right) \,|\, (i,k) \in \mathcal{E}(I_p) \,\} \ .$$

3) **PE for graph signals.** Consider $\mathbf{U}^\epsilon$ as a signal defined on the graph $\mathcal{G}_{\mathbf{U}^\epsilon}$, i.e., $\mathbf{U}^\epsilon \colon \mathcal{V}(\mathcal{G}_{\mathbf{U}^\epsilon}) \longrightarrow \mathbb{R}$ given by $v_{i,j}^\epsilon \hookrightarrow u_{i,j}^\epsilon$.

Definition. *The* multivariate permutation entropy ($\mathrm{MMPE_G}$) *is defined as the permutation entropy* $\mathrm{PE_G}$ *for the graph signal* $\mathbf{U}^\epsilon$ *defined on the graph* $\mathcal{G}_{\mathbf{U}^\epsilon}$*, i.e.,*

$$\mathrm{MMPE_G} = \mathrm{PE_G}(\mathbf{U}^\epsilon) \ .$$

Some remarks of $\mathrm{MMPE_G}$ are the following:

Coarse-grained procedure. The length of each coarse-grained time series is ϵ times shorter than the original one. For $\epsilon = 1$, we get the original series, i.e, $\mathbf{U}^1 = \mathbf{X}$. We use this coarse-grained procedure for simplicity, however other approaches to construct the coarse-graining in multiscale entropy exist [20], [21].

Graph construction associated to a multivariate signal. As an example of the construction, let $\mathbf{X}$ be a multivariate time series with $p = 4$, $n_1 = 6$, $n_2 = n_3 = 7$, $n_4 = 5$ (Fig. 1.a) and full interaction matrix, i.e., $I_p = K_4$ (Fig. 1.b), the graph constructed in Sec. III.2 is shown in Fig. 1.c.

Alternatively, one could match the length of time series by zero-padding to make them suitable for product graphs. However, this approach introduces numerous artificial permutation patterns, which can significantly influence entropy values. Consequently, our method, which avoids this issue, offers a more robust solution.

The graph product, a particular case. When the multivariate signal $\mathbf{X}$ contains series with all equal length, then the

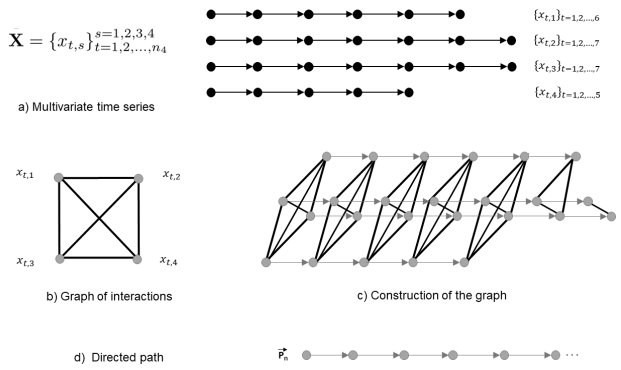

Fig. 1: Graph structures.

previous constructions is the graph product. Formally, the case when $n_p = n$ for all $1, 2, \ldots, p$ implies that $\mathcal{G}_{\mathbf{U}^\epsilon} = \overrightarrow{P}_{\lfloor n/\epsilon \rfloor} \square I_p$, where $\overrightarrow{P}_n$ is the directed path on n vertices (Fig. 1.d). Such particular case was studied previously in [16]. Observe that $\overrightarrow{P}_n$ has adjacency matrix $\mathbf{A}_{\overrightarrow{P}_n}$ (size $n \times n$), and the graph I_p has p vertices with adjacency matrix $\mathbf{A}_{I_p}$ (size $p \times p$), then the adjacency matrix $\mathbf{A}_{\overrightarrow{P}_n \square I_p}$ (size $np \times np$) of the Cartesian product of both graphs $\overrightarrow{P}_n \square I_p$ is given by

$$\mathbf{A}_{\overrightarrow{P}_n \square I_p} = \mathbf{A}_{\overrightarrow{P}_n} \otimes \mathbb{I}_p + \mathbb{I}_n \otimes \mathbf{A}_{I_p} \; ;$$

where $\otimes$ denotes the Kronecker product of matrices and $\mathbb{I}_n$ denotes the $n \times n$ identity matrix.

Graph of interactions. If we consider $I_p = \emptyset$, our method leads to the multiscale multivariate permutation entropy previously presented in [11]. However, $\mathrm{MMPE_G}$ uses information on between channel interaction (represented in the graph I_p) and leads to a more robustness method in the presence of noise, as we will see in the next section.

IV. Robustness to noise

To demonstrate the effectiveness of $\mathrm{MMPE_G}$, we analyse the effect of additive Gaussian noise on its performance on the Lorenz system. This system has important applications in mechanics, biology, and circuit theory [22] and it is given by the system of ordinary differential equations:

$$\begin{aligned} x' &= \sigma(y - x), \\ y' &= x(\rho - z) - y, \\ z' &= xy - \beta z. \end{aligned}$$

A simulation for the values $\rho = 50, \sigma = 19$ and $\beta = 6$, with initial state $x = -1, y = 0$ and $z = 1$ is obtained. We calculate the multivariate permutation entropy, considering two graph structures, I_3 the complete graph with 3 vertices, and I_3' the graph with 3 isolated vertices, and we plot the entropy values as a function of the scale factor ϵ (see Fig. 2). To be noted, that the graph I_3 considers all interaction between channels ($\mathrm{MMPE_G}$) while I_3' does not consider interaction and therefore is the classical MMPE . In both graph structures, the entropy values increase with the scale factor when noise is not added. However, our $\mathrm{MMPE_G}$ shows more stability to the change of scale factor, and the complexity of the multivariate system is more constant, while MMPE [11], [15] shows more variability in its values, changing from no complexity at lower scales to almost random behaviour at higher scales for the same Lorenz system.

To demonstrate the robustness of the method, we add white Gaussian noise to the multivariate signals defined by the Lorenz system. Fig. 2 shows the effects of WGN on multivariate multiscale MMPE and $\mathrm{MMPE_G}$ for the Lorenz system. The signal-to-noise ratio of WGN is set for all the channels as 10dB, 20dB, 30dB, 40dB and 50dB, respectively. The noise has low influence with both methods for scales higher than ten. The influence of the noise is very important for MMPE in lower scales, while the impact is smaller for our algorithm, showing the robustness of $\mathrm{MMPE_G}$.

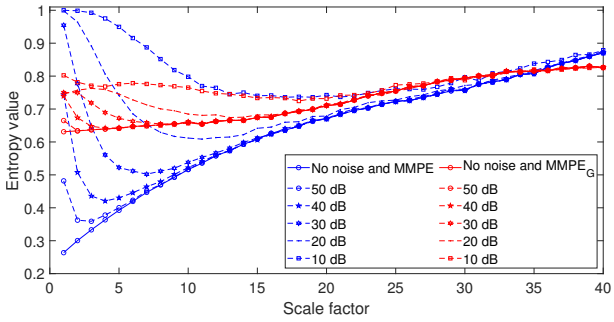

Fig. 2: Entropy values when WGN is added.

Experimental results demonstrate superior performance of $\mathrm{MMPE_G}$ over MMPE when noise is introduced to one, two, or three channels. Furthermore, the addition of a fourth channel consisting solely of noise to the 3-channel Lorentz System does not significantly alter the entropy values. This experiment, which we omit due to space constraints, attests to the robustness of $\mathrm{MMPE_G}$. It is crucial to maintain all channels without deletion when comparing entropy values across different systems with an equal number of channels.

In next section, the robustness of $\mathrm{MMPE_G}$ against noise is validated using more challenging real-world data, specifically two-phase flow data that contains several levels of noise.

V. Flow analysis with $\mathrm{MMPE_G}$

The two-phase flow experiment was carried out at Tianjin University [12], using Electrical Resistance Tomography (ERT). Based on the principle that the conductivity of medium differs, ERT collects boundary voltages between electrodes placed around the pipe by applying electric currents to obtain conductivity distribution of two-phase flow inside the pipe. A constant electrical current of 50 kHz is adopted as the exciting signal, and the data acquisition rate is 120 frames/s. A $16-$electrode ERT obtains $16 \times 13 = 208$ voltage data. Given the redundancy in the measurements and similar to [23], we extract feature vectors V_{Ri} from each electrode to reduce the dimension as follows: $V_{Ri} = \frac{1}{13}\sum_{j=1}^{13}(V_{ij} - V_{ij_0})/V_{ij_0}$ where V_{ij} is the measure voltage value, V_{ij_0} is the V_{ij} when the pipe is full of water and $1 \leq R \leq 16$. Finally, to reduce the computational time, the 16 features vectors V_{Ri} are compressed into 4 time series, by average four V_{Ri} electrode

belonging to the same set group [12]. Then, we applied multivariate multiscale permutation entropy to characterise the two-phase flow.

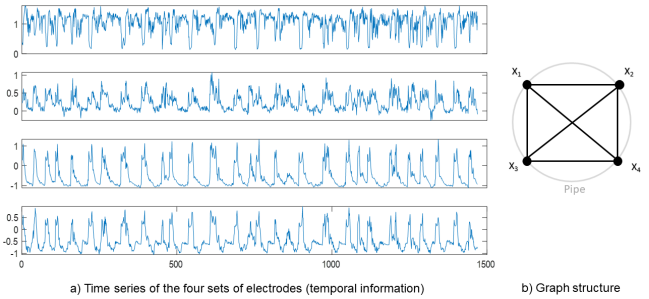

Fig. 3: a) Signals of 4 set of electrodes under annular flow and b) is the graph modelling cross-channel interaction.

Two-phase flow series require preprocessing to eliminate the noise, but our method is noise-robust as shown in Sec. IV and has better results than classical MMPE. Hence we do not need filtering to obtain a good characterisation of the dynamic in phase flow. The noise causes only small variations of entropy values in the lower scales; hence, we will work with the original data without additional preprocessing.

For two-phase flow, gas and water were mixed. Water velocity ranged from 0.4 m/s to 2.9 m/s and gas velocities from 0.06 m/s to 5.64 m/s. The flow pattern observed with this experiments and analysed are patterns known as Bubble flow, Slug flow, Churn flow, and Annular flow. For the analysis, 89 experiments carried out under different conditions of flow rate of gas and water and the typical length of each recording is ∼1400 time samples. We perform the $\mathrm{MMPE_G}$ on the signals of the four flow patterns, and plot the corresponding $\mathrm{MMPE_G}$ versus scale factor in Fig. 4. The coarse-grain process reduces the time series length; consequently, the results show more variability in high-scale factors.

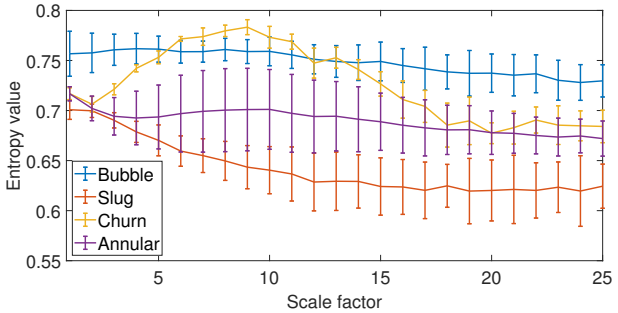

Fig. 4: Mean and standard deviation from $\mathrm{MMPE_G}$ values of signals for different flow patterns.

Entropy of flow patterns. The bubble flow shows the highest $\mathrm{MMPE_G}$ value in almost all scales compared with the other three patterns. The presence of small bubbles [24] in the regime produces complex time series on all four sets of nodes. Because of gravity, the bubbles affect more the top electrodes than the bottom. Then, the high complexity of the time series and different response of the sensors leads to the highest $\mathrm{MMPE_G}$ values.

The signals acquired in slug flow show a periodic fluctuation induced by the repeated occurrence of big gas bubbles. Moreover, the length of the gas bubble could be visually identified in the signal because the four electrode sets are all affected by the big gas bubbles flowing over the measured cross-section and show high voltages resulting from the bubble. Hence, the periodicity on temporal dimension and similar effects in all the electrodes produce the lowest $\mathrm{MMPE_G}$ values for all scales.

The symmetrical distribution of the liquid film around the pipe perimeter in the annular flow leads to the electrodes in the annular flow showing similar fluctuations [25], but with different amplitudes. The liquid film at the bottom of the pipe is thicker than the top due to the gas velocity; see Fig. 3. The complexity depends more on the temporal dimension than the structural dimension. Hence, the values of $\mathrm{MMPE_G}$ overlap in low scales for slug and annular flow, making them indistinguishably but resulting in less complexity than bubble flow. For higher scale, $\mathrm{MMPE_G}$ is able to distinguish between the slug, annular, and bubble flow.

Churn flow is the flow with more dynamic changes along the scale values because it is a highly unstable flow [14]. In lower scales, churn flow is similar to the slug and annular flow. The presence of bubbles in the churn flow and the interaction and coalesce with each other produces the highest entropy values than slug and annular flow for scales between 3-14 and more complexity than bubble for scales between 7-11 because of the presence of no complete slugs and small waves. Periodic waves are relevant for higher scales, decreasing the values of $\mathrm{MMPE_G}$ and making them similar to the annular flow.

Alternative graph structures: As each channel is represented by a vertex, we considered all possible non-isomorphic simple graphs I_p with four vertices, resulting in 11 graphs. Out of these, five are disconnected (G1-G5) and six are connected graphs (G6-G11). Our results showed that *connected graphs* exhibit better performance in characterizing two-phase flow than *disconnected graphs*, as they produce more stable entropy values, with less variance and overlap between different phase-flows across the multiscale values.

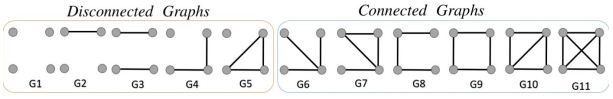

Fig. 5: All non-isomorphic graphs with four vertices.

Disconnected Graphs. The performance of $\mathrm{MMPE_G}$ is more variable when the underlying graph is one of the five disconnected graphs, with I_P=G1 showing the best performance. This is due to the lack of edges and equal consideration of all signals. This scenario leads to the classical multivariate multiscale permutation entropy, as shown in Fig. 6, where the results in overlap across almost all multiscale values, making it difficult to difference flow patterns.

Connected Graphs. Our results show that the complete graph G11, the chosen default graph, outperforms the other connected graphs, as G11 has the most edges (six) which results in more interchannel dependencies being considered.

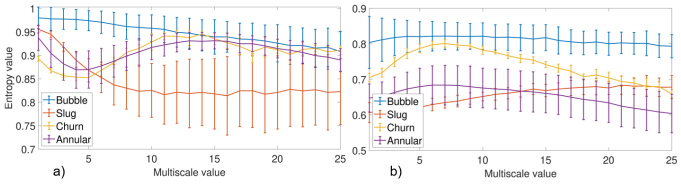

Fig. 6: Entropy values when the graph is (a) G1 and (b) G9.

The multiscale incorporates time dependency and the graph G11 considers variations between close vertices (sensors), thereby capturing dynamic behaviour in a more effective manner. The cycle graph G9 also has good performance, clearly distinguishing bubble flow from others, but not annular from slug flow (Fig. 6) because the information considered in the graph being only boundary information (modelled by the cycle graph) and inner information being missing (represented by the complement).

This highlights the advantage of using the G1 or G11 when there is no additional information and a small number of channels. Additionally, both graphs are the only ones that do not depend on which vertex corresponds to each time series.

When the graph is large, it becomes more appropriate to consider information about the system. For example, if data is compressed into 16, rather than four time series [23], the complete graph will have 120 edges or channel dependencies, making difficult detect the dynamics (Fig. 7(b)). In this case, information such as the localization of the sensors, modelled by a cycle graph with 16 vertices, will produce better results (Fig. 7(a)) but increase the computational time.

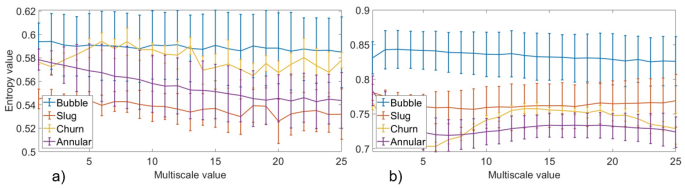

Fig. 7: Entropy values for 16 time series, with underlying graph: a) the complete graph (K_{16}) and b) a cycle graph (C_{16}).

VI. Conclusions

This paper proposes a multiscale methodology to analyse multivariate time series (with unequal lengths) using the concept of permutation entropy. Contrary to the previous state of the art, our method allows for the consideration of cross-channel interactions, thanks to the exploitation of graph products and our recent formulation of permutation entropy for graph signals. Our proposed approach provides a robust and effective method for analysing the complexity of multivariate time series, characterising complex systems (including two-phase flow recordings) and make it a valuable tool in a range of fields, including signal analysis and industrial process analysis.

References

[1] S. Levy, *Two-phase flow in complex systems*. John Wiley & Sons, 1999.

[2] D. Drew, "Mathematical modeling of two-phase flow," *Annual review of fluid mechanics*, vol. 15, no. 1, pp. 261–291, 1983.

[3] H. B. Stewart and B. Wendroff, "Two-phase flow: models and methods," *Journal of Computational Physics*, vol. 56, no. 3, pp. 363–409, 1984.

[4] H. Li, Y. Zhou, B. Sun, and Y. Yang, "Multi-scale chaotic analysis of the characteristics of gas-liquid two-phase flow patterns," *Chinese Journal of Chemical Engineering*, vol. 18, no. 5, pp. 880–888, 2010.

[5] C. Bandt and B. Pompe, "Permutation entropy: a natural complexity measure for time series," *Physical review letters*, vol. 88, no. 17, p. 174102, 2002.

[6] I. Veisi, N. Pariz, and A. Karimpour, "Fast and robust detection of epilepsy in noisy EEG signals using permutation entropy," in *IEEE (BIBE)*, 2007, pp. 200–203.

[7] C. Fan, N. Jin, X. Chen, and Z. Gao, "Multi-scale permutation entropy: A complexity measure for discriminating two-phase flow dynamics," *Chinese Physics Letters*, vol. 30, no. 9, p. 090501, 2013.

[8] A. Dàvalos, M. Jabloun, P. Ravier, and O. Buttelli, "Multiscale permutation entropy: Statistical characterization on autoregressive and moving average processes," in *EUSIPCO 2019*, 2019, pp. 1–5.

[9] M. Ahmed and D. P. Mandic, "Multivariate multiscale entropy: A tool for complexity analysis of multichannel data," *Physical Review E*, vol. 84, no. 6, p. 061918, 2011.

[10] H. Azami, A. Fernández, and J. Escudero, "Multivariate multiscale dispersion entropy of biomedical times series," *Entropy*, vol. 21, no. 9, p. 913, 2019.

[11] F. Morabito, D. Labate, F. Foresta, A. Bramanti, G. Morabito, and I. Palamara, "Multivariate multi-scale permutation entropy for complexity analysis of Alzheimer's disease EEG," *Entropy*, vol. 14, no. 7, pp. 1186–1202, 2012.

[12] C. Tan, J. Zhao, and F. Dong, "Gas–water two-phase flow characterization with electrical resistance tomography and multivariate multiscale entropy analysis," *ISA transactions*, vol. 55, pp. 241–249, 2015.

[13] Z. Gao, M. Ding, H. Geng, and N. Jin, "Multivariate multiscale entropy analysis of horizontal oil–water two-phase flow," *Physica A: Statistical Mechanics and Its Applications*, vol. 417, pp. 7–17, 2015.

[14] Z. Gao, Y. Yang, L. Zhai, M. Ding, and N. Jin, "Characterizing slug to churn flow transition by using multivariate pseudo wigner distribution and multivariate multiscale entropy," *Chemical Engineering Journal*, vol. 291, pp. 74–81, 2016.

[15] Y. Yin and P. Shang, "Multivariate weighted multiscale permutation entropy for complex time series," *Nonlinear Dynamics*, vol. 88, no. 3, pp. 1707–1722, 2017.

[16] J. Fabila-Carrasco, C. Tan, and J. Escudero, "Multivariate permutation entropy, a Cartesian graph product approach," in *EUSIPCO*, 2022.

[17] ——, "Permutation entropy for graph signals," *IEEE Transactions on Signal and Information Processing over Networks*, vol. 8, pp. 288–300, 2022.

[18] S. Kadambari and S. Chepuri, "Learning product graphs from multidomain signals," in *ICASSP*, 2020, pp. 5665–5669.

[19] J. Fabila-Carrasco, "The discrete magnetic laplacian: geometric and spectral preorders with applications," Ph.D. dissertation, Universidad Carlos III de Madrid, 2020.

[20] H. Azami and J. Escudero, "Coarse-graining approaches in univariate multiscale sample and dispersion entropy," *Entropy*, vol. 20, no. 2, p. 138, 2018.

[21] J. Valencia, A. Porta, M. Vallverdu, F. Claria, R. Baranowski, E. Orlowska-Baranowska, and P. Caminal, "Refined multiscale entropy: Application to 24-h holter recordings of heart period variability in healthy and aortic stenosis subjects," *IEEE Transactions on Biomedical Engineering*, vol. 56, no. 9, pp. 2202–2213, 2009.

[22] M. Hirsch, S. Smale, and R. Devaney, *Differential equations, dynamical systems, and an introduction to chaos*. Academic press, 2012.

[23] C. Tan, Y. Shen, K. Smith, F. Dong, and J. Escudero, "Gas–liquid flow pattern analysis based on graph connectivity and graph-variate dynamic connectivity of ERT," *IEEE Transactions on Instrumentation and Measurement*, vol. 68, no. 5, pp. 1590–1601, 2018.

[24] X. Dong, C. Tan, and F. Dong, "Gas–liquid two-phase flow velocity measurement with continuous wave ultrasonic doppler and conductance sensor," *IEEE Transactions on Instrumentation and Measurement*, vol. 66, no. 11, pp. 3064–3076, 2017.

[25] C. Tan, W. Dai, H. Yeung, and F. Dong, "A Kalman estimation based oil–water two-phase flow measurement with CRCC," *International Journal of Multiphase Flow*, vol. 72, pp. 306–317, 2015.